# Microwave Zeeman Effect of Free Hydroxyl Radicals*

H. E. RADFORD
*National Bureau of Standards, Washington, D. C.*
(Received November 7, 1960)

Paramagnetic resonance absorption at 3-cm wavelength has been observed in the products of an electric discharge in low-pressure $H_2O$ and $D_2O$ vapor. The spectra are of the electric dipole type, and arise from $\Lambda$-type doubling transitions in low-lying rotational levels of the free $O^{16}H$ and $O^{16}D$ radicals. The theory of the Zeeman effect in $^2\Pi$ levels of light diatomic radicals is extended to the general intermediate coupling case, and is used for a detailed analysis of the observed spectra. Numerical results of this analysis include molecular $g$ factors precise to within 3 parts in $10^5$, and magnitudes of the $\Lambda$-type doubling intervals in several low rotational levels. The measured $g$ factors are compared with theory, including small corrections for molecular rotation, the anomalous spin magnetic moment of the electron, and estimated relativistic effects. This comparison yields the value $0.67\pm0.01$ for the molecular matrix element $(\Pi|L_y|\Sigma)$, and also brings to light serious discrepancies between the present experimental results and earlier measurements of the $\Lambda$-type doubling in OH and OD. The paramagnetic resonance spectra also exhibit hyperfine structure, from which are derived molecular constants that describe the distribution of unpaired electrons about the H or D nucleus.

## I. INTRODUCTION

EXPERIMENTS by Dousmanis, Sanders, and Townes[1] (hereafter referred to as DST) and by Ehrenstein, Townes, and Stevenson[2] have demonstrated microwave resonance absorption by the free hydroxyl radicals OH and OD in the products of an electric discharge in water vapor. Their work was concerned with the measurement and interpretation of small splittings of the molecular energy levels, the so-called $\Lambda$-type doubling intervals, as well as a partial measurement of the magnetic dipole hyperfine structure. These were straight microwave absorption experiments, done in the absence of external fields. The experiment to be described here is quite similar to this earlier work, the essential difference being the application of a steady magnetic field to the gaseous absorption sample; this reveals the Zeeman effect of the $\Lambda$-type doubling absorption. Hydroxyl radicals possess a paramagnetic $^2\Pi$ ground state; hence the Zeeman effect is large, and standard paramagnetic resonance absorption techniques are applicable. We have used a commercial $X$-band spectrometer to measure the Zeeman effect, hyperfine structure, and $\Lambda$-type doubling in several low rotational levels of OH and OD. The same apparatus, widely available, can also be used for chemical studies of hydroxyl radicals in gases; the results of a few qualitative investigations of this sort are also given here.

Our major objective was to measure the molecular Zeeman effect and then to compare it with theory. As in similar investigations of free paramagnetic atoms,[3] this comparison can test the finer details of the Zeeman theory, including the small quantum electrodynamic correction for the anomalous spin magnetic moment of the electron. The validity of this correction to the atomic Zeeman theory has been amply demonstrated by several precise measurements of atomic $g$ factors. In extending the calculation of the quantum electrodynamic correction from atoms to diatomic molecules, one tacitly assumes that the basic change in the symmetry of the system—from the spherical symmetry of an atom to the axial symmetry of a diatomic molecule—introduces no difficulties more subtle than can be accounted for by ordinary vector coupling rules. This is the aspect of the theory that requires an experimental test.

Three independent magnetic resonance measurements on the diatomic oxygen molecule have given somewhat contradictory evidence on this point. The magnetic properties of oxygen are chiefly those of its two unpaired electrons, coupled by a weak spin-spin interaction. From the resonance experiments one can deduce a value of $g_s(O_2)$, the spin $g$ factor of the coupled two-electron system. Apart from possible small relativistic corrections for binding of the electrons in the molecule, this value should be equal, if the theory is correct, to $g_s$(free), the anomalous spin $g$ factor of a single free electron; the numerical value of the latter is 2.00232. The results of the first experiment, a strong-field paramagnetic resonance investigation of oxygen gas,[4] confirmed the equality of $g_s(O_2)$ and $g_s$(free) within the experimental precision of 60 parts in $10^6$. The second experiment, performed at low field strengths by the molecular beam magnetic resonance method,[5] indicated that $g_s(O_2)$ was smaller than $g_s$(free) by $190\pm13$ parts in $10^6$. The third and latest experiment, a more precise reinvestigation of the strong-field

* This work was supported by the Office of Naval Research.
[1] G. C. Dousmanis, T. M. Sanders, Jr., and C. H. Townes, Phys. Rev. **100**, 1735 (1955). Referred to throughout this paper as DST.
[2] G. Ehrenstein, C. H. Townes, and M. J. Stevenson, Phys. Rev. Letters **3**, 40 (1959).
[3] A recent review of atomic magnetism is given by V. W. Hughes, in *Recent Research in Molecular Beams* (Academic Press, Inc., New York, 1959); an extensive bibliography is included.
[4] M. Tinkham and M. W. P. Strandberg, Phys. Rev. **97**, 951 (1955).
[5] J. M. Hendrie and P. Kusch, Phys. Rev. **107**, 716 (1957).

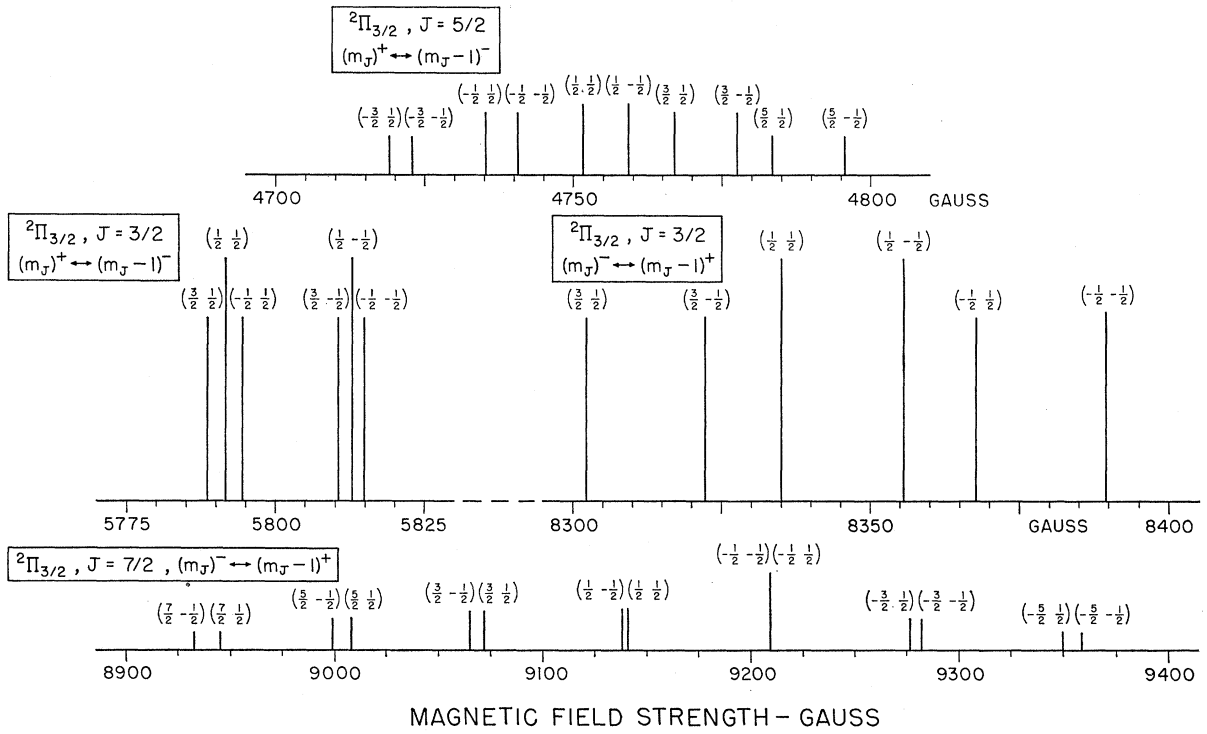


FIG. 1. Paramagnetic resonance spectra of $O^{16}H$. Microwave frequency: 9263 Mc/sec. Note change of scale in bottom spectrum. The labelling scheme used to identify the lines is $(m_J,m_I)$.

paramagnetic resonance spectrum,[6] gave this difference to be $147\pm10$ parts in $10^6$. Thus all three experiments appear to show the quantum electrodynamic effect, but fail to agree on its magnitude. There are other discrepancies: the experiments gave different values for the molecular rotational magnetic moment, and the magnitude of the quadratic Zeeman effect observed in the molecular beam experiment differed appreciably from the theoretical prediction.

The paramagnetic gas nitric oxide has also been studied in a strong-field paramagnetic resonance experiment.[7] The magnetic properties of this diatomic molecule are produced by a single unpaired electron, having both spin and orbital angular momentum. To extract a value of the spin $g$ factor $g_s(\mathrm{NO})$ from the observed spectrum, one requires precise knowledge of the vector coupling scheme; this is specified by a single coupling parameter, which may be measured by standard spectroscopic methods. Using the optically measured value of this parameter, one finds[8] in the paramagnetic resonance spectrum no evidence for the anomalous part of the electron spin moment; that is, the spectrum is accounted for much better by the value $g_s(\mathrm{NO})=2.0000$ than by $g_s(\mathrm{NO})=g_s(\mathrm{free})=2.00232$.

Very recently, the nitric oxide spectrum has been reinterpreted with a different and more precise value of the coupling parameter, measured by microwave spectroscopy. The paramagnetic resonance spectrum is now found to be consistent, to a precision of about one part in $10^4$, with the value $g_s(\mathrm{NO})=g_s(\mathrm{free})$.[9]

The history of the nitric oxide work is mirrored in a curious way by the results of the present experiment. The hydroxyl radicals OH and OD are similar in electronic structure to nitric oxide, and the correct interpretation of their paramagnetic resonance spectra also requires accurate knowledge of the vector coupling schemes. Again the necessary coupling parameters have been measured both in optical and microwave experiments (the latter being the experiment of DST); the optical values again differ somewhat from the presumably more accurate microwave values. In this case, however, the observed spectra are consistent with $g_s(\mathrm{OH})=g_s(\mathrm{OD})=g_s(\mathrm{free})$ when the *optical* values of the coupling parameters are used in the analysis; the microwave values of these parameters yield the result $g_s(\mathrm{OH})=g_s(\mathrm{OD})=2.0000\pm0.0002$, the same value indicated for $g_s(\mathrm{NO})$ by the first interpretation of the nitric oxide experiment.

Thus, on the basis of these two experiments alone, one would be hard put to decide whether an electron in a diatomic molecule showed its full anomalous magnetic moment or whether, for some unexpected

[6] K. D. Bowers, R. A. Kamper, and C. D. Lustig, Proc. Roy. Soc. (London) **A251**, 565 (1959).

[7] R. Beringer and J. G. Castle, Jr., Phys. Rev. **78**, 581 (1950); R. Beringer, E. B. Rawson, and A. F. Henry, Phys. Rev. **94**, 343 (1954).

[8] C. C. Lin and M. Mizushima, Phys. Rev. **100**, 1726 (1955).

[9] C. C. Lin, Phys. Rev. **119**, 1027 (1960).

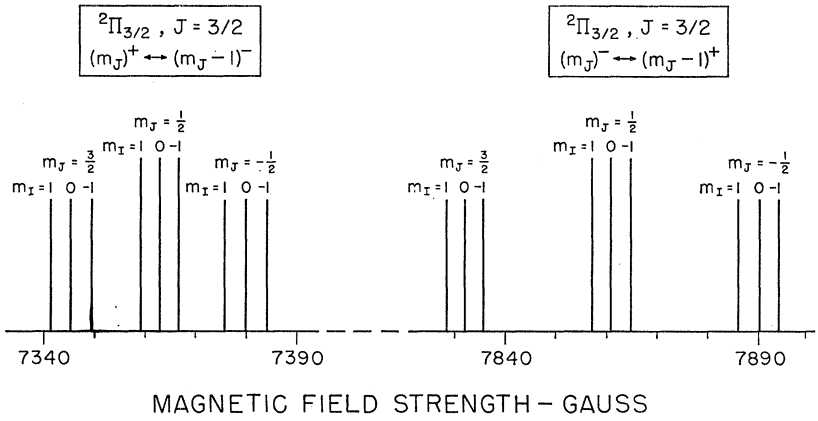


FIG. 2. Paramagnetic resonance spectrum of $O^{16}D$. Microwave frequency: 9475 Mc/sec.

reason, it showed only the Dirac part of its moment. In view of the further evidence provided by the oxygen experiments, it is probably most reasonable to conclude that the anomalous part of the electron spin moment does in fact contribute to the hydroxyl radical Zeeman effect, but that in the analysis of the paramagnetic resonance spectra this contribution is completely masked by errors in the DST values of the coupling parameters.

## II. EXPERIMENT

The products of an electric discharge in low-pressure $H_2O$ vapor were pumped continuously through the microwave cavity of a Varian V-4500 EPR spectrometer, where the microwave absorption by the vapor at 3-cm wavelength was measured as a function of magnetic field strength. The magnetic field was provided by a Varian 12-inch electromagnet, whose maximum field strength was 11 kgauss. Many discrete absorption lines were observed, some of which could be identified by gas substitution methods with molecular oxygen, atomic oxygen, and atomic hydrogen. The remaining lines, those that disappeared when the water vapor input was replaced by either dry oxygen or dry hydrogen, with the electric discharge either on or off, are represented in Fig. 1. The source of $H_2O$ vapor was ordinary distilled water; when this was replaced by a water sample containing 95% $D_2O$, the intensities of the spectra in Fig. 1 decreased proportionately and the new spectrum of Fig. 2 appeared. Since an electric discharge in water vapor is known to be a good source of hydroxyl radicals,[1] it is reasonable to identify the spectra of Fig. 1 with free OH radicals, the spectrum of Fig. 2 with free OD radicals; this identification is confirmed by the detailed analysis of Sec. III below.

The arrangement of the gas handling system, absorption cell, and spectrometer cavity is shown in Fig. 3. The cavity is a circular cylindrical reflection cavity, silver plated and fitted with removable end plates. The dimensions of the cavity are chosen to make it resonate in the $TE_{102}$ mode. Its volume is rather large, about 100 cm$^3$; this helps to alleviate power saturation of the absorption lines by keeping the microwave field intensities low. The end plates are drilled to pass the radical vapor tube, and have collars that prevent leakage of the cavity radiation. The absorption cell has a pillbox shape and fits snugly into the cavity; it is made of quartz to minimize dielectric losses. With the quartz cell in place the cavity $Q$ is $6\times10^3$, approximately half that of the empty cavity.

The radical vapor is pumped through the absorption cell by a high-conductance liquid nitrogen trap and a 6-liter/sec mechanical pump. A mechanical manometer measures pressure at the vapor inlet point; a thermocouple gauge located near the exit aperture of the absorption cell gives a rough indication of pressures within the cell. Sufficient production of radicals requires a pressure in the electric discharge of at least 0.3 mm Hg, while for satisfactory resolution of the pressure-broadened absorption lines the pressure at the absorption cell must be less than 0.1 mm Hg. Such a pressure differential is maintained by the long (1.5 m), low-conductance (1 cm i.d.) quartz tube that separates the electric discharge from the absorption cell. This extended arrangement, made feasible by the rather long lifetime of hydroxyl radicals in water vapor, has other advantages: it reduces electrical interference between the discharge and the spectrometer detection circuits, and it guarantees that the free-electron content of the radical vapor has become negligible by the time the vapor reaches the absorption cell. The latter point is more important than it might seem, for in early measurements[10] the spectrum labelled $^2\Pi_{\frac{3}{2}}$, $J=\frac{5}{2}$ in Fig. 1 was almost completely obscured by an extremely broad and intense absorption, centered at 3300 gauss, caused by cyclotron resonance of free electrons within the absorption cell. At that time the electric discharge was located about 20 cm away from the absorption cell; increasing the separation to 50 cm or more removed the difficulty. There is no serious loss of O, H, or OH radicals during the extended trip to the absorption cell, although the transit time is as

[10] H. E. Radford, Nuovo cimento 14, 245 (1959).

much as 0.1 sec over the full 1.5-m distance. The only wall treatment applied to the long tube and absorption cell was a thorough washing with detergent, followed by rinses with 20% HF solution and distilled water.

The electric discharge is excited by a waveguide resonator that can be placed over the vapor tube at any desired point along its length; a diathermy generator supplies 2450 Mc/sec power to the discharge resonator at a variable level up to 125 watts. For a given inlet vapor pressure, it was usually possible to maximize the radical concentration in the absorption cell (as judged by absorption signal amplitudes) by adjusting the power level and the position of the resonator. The intensity of the maximized absorption signal increased rapidly as the inlet pressure was raised to about 2 mm Hg, and fell off slowly as the pressure was raised further. Since in a heterogeneous vapor the peak absorption intensity of a pressure-broadened line should depend on the fractional concentration of the absorbing species, this variation presumably reflected a changing dissociation efficiency in the discharge.

Under optimum pressure and discharge conditions the hydroxyl radical absorption signals are very strong; with an appropriate magnetic field sweep and wide-band signal amplification, it is possible to display one or more of the absorption lines directly on the screen of an oscilloscope. From this video display, the instantaneous concentration of hydroxyl radicals in the absorption cell can be monitored. Atomic hydrogen and atomic oxygen are also produced in large quantities in the water vapor discharge, and their concentrations may be monitored in the same way. The molecular oxygen absorption lines are too weak for a video presentation.

A section of the radical vapor tube in Fig. 3 is bent to a U shape to fit into a Dewar flask; it was used for the following temperature studies of the water vapor discharge products.

*Fractional condensation.* Hydrogen atoms, oxygen atoms, and hydroxyl radicals are all condensed (i.e., fail to get through the trap) at liquid nitrogen temperature; hydroxyl radicals are condensed at dry ice temperature but atomic oxygen and atomic hydrogen are not. These conclusions are based on a video display of the absorption lines: the lines, whose amplitudes were at least 10 times the noise level at the start, vanished immediately and completely when the U trap was cooled. A more detailed investigation, using a variable temperature pentane bath and pen recording of the absorption line, showed that 70% of the hydroxyl radicals were condensed at a temperature of $-60°C$, 95% were condensed at $-90°C$.

*Hydroxyl radical linewidth.* With the pressure and discharge conditions set to give the maximum fractional concentration of hydroxyl radicals, the absorption lines were pressure-broadened to a width of about 5 Mc/sec. As the hydroxyl radical concentration was progressively reduced by lowering the trap temperature from 20°C to $-90°C$, there was no measureable change in the absorption linewidth. This demonstrates that pressure broadening of the hydroxyl radical lines is caused by other vapor fractions uncondensible at $-90°C$ (i.e., H, O, $O_2$, $H_2$), and that these uncondensible fractions are the major products of the water vapor discharge, probably constituting 90% or more of the radical vapor in the spectrometer cavity.

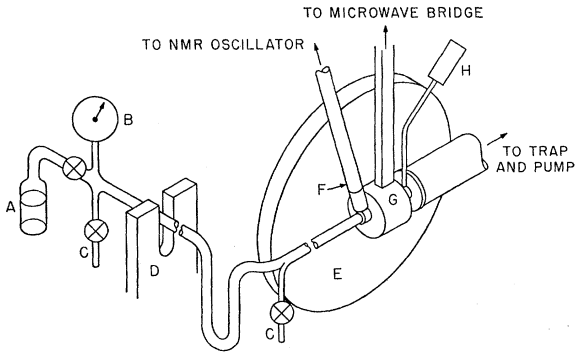


FIG. 3. Gas handling system and spectrometer cavity. A: $H_2O$ or $D_2O$ sample vial; B: Wallace & Tiernan vacuum gauge; C: inlet for admixing foreign gases to vapor stream; D: waveguide discharge resonator; E: pole face of electromagnet; F: nuclear magnetic resonance probe; G: spectrometer microwave cavity ($TE_{012}$, 3 cm); H: thermocouple vacuum gauge.

Several attempts were made to increase the fractional concentration of hydroxyl radicals produced by the discharge; these included replacing the water sample by hydrogen peroxide or a stoichiometric mixture of hydrogen and oxygen gas, adding various gases ($H_2$, $N_2$, $O_2$, He, Ar) to the vapor stream either before or after the water vapor discharge, and adding a small amount of water vapor to a noble gas discharge. With one exception, all of these attempts failed. The exception was the addition of oxygen gas to the water vapor before the discharge: this enhanced the fractional concentration of hydroxyl radicals by as much as a factor of two when the initial water vapor pressure was rather high, 2–4 mm Hg at the inlet, but the enhancement decreased with vapor pressure, becoming negligible for an inlet pressure of 0.5 mm Hg or so.

For precise line position measurements on the spectra of Figs. 1 and 2, the absorption signals, modulated by a small 1-kc/sec modulation of the magnetic field, were passed through the narrow band amplifier and synchronous detector of the Varian instrument and displayed, in derivative form, on a strip chart recorder. Signal-to-noise ratios of about 400 could be realized on the strongest lines under conditions of optimum radical production; however, most of this signal strength was sacrificed in favor of the reduction in linewidth that accompanied low-pressure (and inefficient) operation of the discharge. For the strongest lines the pressure at the absorption cell could be reduced to the point where the thermocouple gauge indicated 50 $\mu$Hg.

At this pressure the width between derivative maxima was 450 kc/sec (0.35 gauss) and the signal-to-noise ratio was about 10. The weaker lines of Fig. 1 required pressures as high as 100 $\mu$Hg for satisfactory detection, and at this pressure the linewidth was 800 kc/sec. In order to avoid further broadening of the lines through microwave power saturation, the power feed to the cavity had to be kept lower than 5 microwatts.

The location of a given line was determined by successive measurements of the microwave frequency and of the magnetic field strength at the line center. The microwave frequency measurements, made with a Hewlett-Packard transfer oscillator and electronic frequency counter, were precise to 1 part in $10^6$. The magnetic field was measured in terms of the nuclear magnetic resonance frequency of protons or (for field strengths above 8.5 kgauss) $Li^7$ nuclei, both contained in an aqueous solution of lithium nitrate. The resonance circuit was a free-running Pound-Knight-Watkins oscillator,[11] whose frequency was monitored by the same frequency counter as used for the microwave measurement. The magnetic field was measured at a point just outside the microwave cavity, and field measurements were corrected for the small ($\sim$0.05 gauss) field differential, remeasured periodically, that existed between the position of the magnetometer probe and the cavity center.

The hydroxyl radical absorption lines were 1 part in $10^4$ or less in relative width, and had the symmetric Lorentz shape expected from pure collision broadening. Although the attainable precision of position measurements on such lines may approach 1 part in $10^6$ (as given by the statistical standard error in the mean result of several observations), no attempt was made to achieve this extreme precision. As will be evident from the discussion in Sec. IV, an experimental precision poorer by an order of magnitude is more than adequate for a comparison of theory with experiment. The experimental results given in Table II are derived from two or three independent position measurements on each line in the spectra of Fig. 1 and Fig. 2. Adopting as a conventional index of precision the tenth part of the linewidth, and doubling this figure in recognition of possible systematic errors in the magnetic field measurements, we believe a conservative limit for experimental errors to be $\pm 2$ parts in $10^5$. The uncertainties quoted in Table II are based on this estimate.

## III. THEORY

We seek to assign the spectra of Fig. 1 and Fig. 2 to transitions among the magnetic sublevels of the free OH and OD radicals. These sublevels are eigenvalues of the molecular Hamiltonian

$$H = H_0 + Z + H_{\text{hfs}},$$

in which $H_0$ includes the electrostatic, vibrational, rotational, and fine structure interactions, $Z$ is the Zeeman operator, and $H_{\text{hfs}}$ is the hyperfine structure (hfs) operator. Detailed expressions for $Z$ and $H_{\text{hfs}}$ are given below.

On the reasonable assumption that the radical vapor is in thermal equilibrium with the walls of the absorption cell, only the ground electrostatic-vibrational molecular term will be populated appreciably. Furthermore, only the lowest fine structure-rotational levels of this ground term have magnetic moments large enough to account for the observed paramagnetic resonance spectra. The disposition of these lowest levels for both OH [12] and OD,[13] determined by ultraviolet spectroscopy, is shown in Fig. 4. The $\Lambda$-type doubling of each level is exaggerated for clarity; many of these splittings, barely detectable by optical means, were measured to high precision in the zero-field microwave absorption experiments.[1,2] In the following sections, general expressions are developed for the Zeeman effect and hfs of all these lower levels. The comparison of these results with the observed paramagnetic resonance spectra serve to identify the spectra, and also to determine the values of unknown molecular constants used in the calculation.

Compared with the separations between levels in Fig. 4, the expected Zeeman and hfs splittings of each

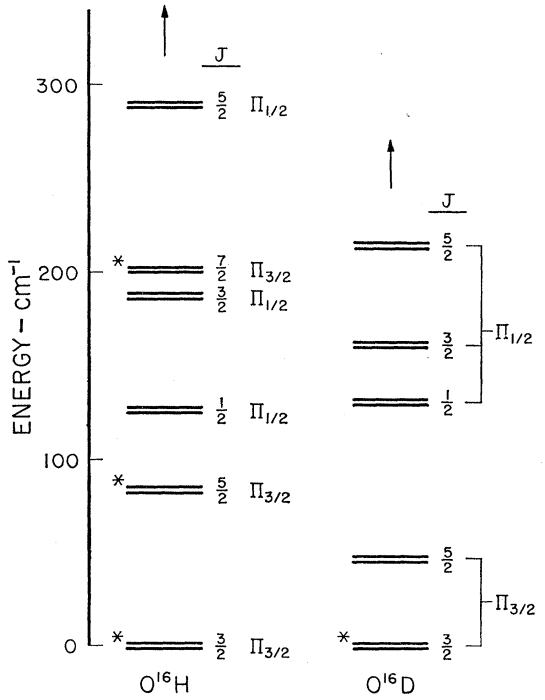


FIG. 4. Lowest fine structure-rotational levels of $O^{16}H$ and $O^{16}D$. The small $\Lambda$-type doubling intervals are exaggerated for clarity. Levels marked with asterisks contribute to the paramagnetic resonance spectra of Figs. 1 and 2.

[11] G. D. Watkins and R. V. Pound, Phys. Rev. **82**, 343 (1951).

[12] G. H. Dieke and R. M. Crosswhite, Bumblebee Report No. 87, Johns Hopkins University, November, 1948 (unpublished).

[13] M. Ishaq, Proc. Roy. Soc. (London) **159**, 110 (1937).

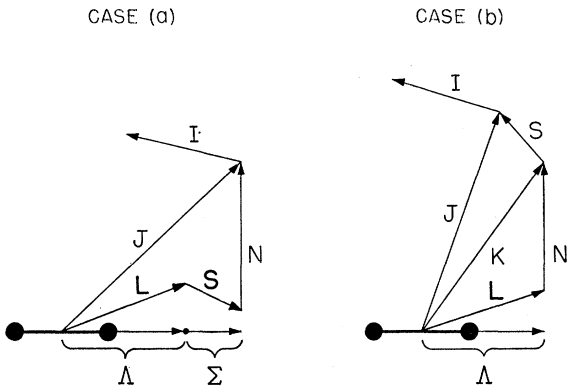


FIG. 5. Vector coupling diagrams for Hund's case (a) and case (b) under strong-field conditions (negligible hyperfine couplings).

level are very small—typically 0.1 $cm^{-1}$ for the Zeeman splittings and 0.001 $cm^{-1}$ or less for the hfs splittings. This suggests the feasibility of a straightforward perturbation calculation of the Zeeman effect and hfs, starting from the zero order energies and wave functions defined by $H_0\psi_0=W_0\psi_0$. Because the hfs energies are in all cases much smaller than the Zeeman energies, it is permissible to treat the two perturbations entirely separately; this means that the perturbation calculation of the molecular Zeeman effect can be carried out with a pure strong-field representation of the zero order wave functions, i.e., a representation that takes no account of hyperfine interactions. The first-order hfs energies can then be calculated in this representation and simply added to the Zeeman energies.

## 1. The Molecular Zeeman Effect

The Zeeman operator is

$$Z=\mu_0(g_l\mathbf{L}+g_s\mathbf{S}+g_I\mathbf{I}+g_N\mathbf{N})\cdot\mathfrak{H}, \qquad (1)$$

where **L** and **S** are the electronic orbital and spin angular momenta, **I** is the spin of the proton in OH or of the deuteron in OD, and **N** is the end-over-end rotational angular momentum of the molecule; all are expressed in units of $\hbar$. Strictly, the rotational term is to be evaluated only for the two bare nuclei; all electronic contributions to the Zeeman effect are embraced by the first two terms of $Z$. The electronic $g$ factors $g_l$ and $g_s$ are, from theory, $g_l=1$ and $g_s=2(1+\alpha/2\pi-0.328\alpha^2/\pi^2)=2(1.0011596)$[14]; these values have been verified to within a few parts in $10^6$ by experiment.[3,15] The nuclear spin $g$ factors are defined here by the relation $g_I=-\mu_I/I\mu_0$ where $\mu_I$ is the measured nuclear spin magnetic moment and $I$ is the nuclear spin quantum number; numerical values are $g_I(\mathrm{H})=-3.042\times10^{-3}$ and $g_I(\mathrm{D})=-4.67\times10^{-4}$. The nuclear rotational $g$ factor is defined in a similar way as $g_N=-\mu_N/N\mu_0$ and it may be calculated by giving $\mu_N$ and **N** their classical interpretations as the magnetic moment and angular momentum of a charged dumbbell rotator. For a proton or deuteron rotating about a fixed oxygen nucleus the $g$ factor would be $-(Z/A)(m/M)$, where $Z/A$ is the ratio of charge and mass numbers for the rotating nucleus, equal to 1 for OH and $\frac{1}{2}$ for OD. If the small relative motion of the oxygen nucleus is included, the $g$ factors become

$$g_N(\mathrm{OH})=-0.996m/M=-5.42\times10^{-4}$$

and

$$g_N(\mathrm{OD})=-0.500m/M=-2.72\times10^{-4}.$$

Although the theoretical value of $g_s$ contains a small correction term of order $\alpha^2$ $[=(137)^{-2}]$, the Zeeman operator above cannot be considered correct to the same order: relativistic interaction terms contribute in order $\alpha^2\mu_0\mathfrak{H}$ to the Zeeman energies of atoms,[3] and similar contributions can be expected for diatomic molecules. The further discussion of this point in Sec. V indicates that the nonrelativistic operator (1) will generate Zeeman energies that, for the hydroxyl radicals, err on the large side by 1 or 2 parts in $10^4$.

### *1.1 The Linear Zeeman Effect*

By far the largest contribution to the molecular Zeeman energies comes from the first order term $(\psi_0|Z|\psi_0)$, the expectation value of the Zeeman operator in the zero-order state. Its accurate calculation requires a rather careful representation of the zero-order wave functions.

*Wave functions.* Since $Z$ contains only angular momentum operators, we require precise knowledge of only the angular dependence of the zero-order molecular wave functions. This angular dependence may be represented in the usual way by an expansion in suitably chosen base functions, the expansion coefficients to be determined ultimately by experiment. The vector model of diatomic molecules defines several sets of base functions, each set corresponding to a different pure coupling case[16]; spectroscopic studies show that most diatomic molecules are pretty good examples of one pure coupling case or another, and so their wave functions can be represented for most purposes by single base functions. Nitric oxide for example, is a good Hund's case (a) molecule[17]: both **L** and **S** are coupled tightly to the molecular axis—**L** by its electrostatic coupling with the internuclear field, **S** by its spin-orbit coupling with **L**. The strong-field base functions, written in terms of their well-defined quantum numbers, are $|\Lambda\,\Sigma\,\Omega\,S\,J\,I\,m_J\,m_I)$, where $\Lambda$, $\Sigma$, and $\Omega$ are the projections of **L**, **S**, and **J** on the molecular axis, and $m_J$ and $m_I$ are the projections of

[14] C. M. Sommerfield, Phys. Rev. **107**, 328 (1957); Ann. Phys. **5**, 26 (1958).

[15] A. A. Schupp, R. W. Pidd, and H. R. Crane, Phys. Rev. **121**, 1 (1961).

[16] G. Herzberg, *Molecular Spectra and Molecular Structure* (D. Van Nostrand Company, Inc., New York, 1950), Vol. 1, p. 219.

[17] See reference 16 for a complete discussion of Hund's coupling cases.

TABLE I. Strong-field case (a) base functions.

| $\|\Lambda\,\Sigma\,\Omega\,S\,J\,I\,m_J\,m_I\rangle$ | Spectroscopic notation |
|---|---|
| $\|1\,\frac{1}{2}\,\frac{3}{2}\,\frac{1}{2}\,J\,I\,m_J\,m_I\rangle$ | $^2\Pi_{\frac{3}{2}}$ |
| $\|-1\,-\frac{1}{2}\,-\frac{3}{2}\,\frac{1}{2}\,J\,I\,m_J\,m_I\rangle$ | $^2\Pi_{-\frac{3}{2}}$ |
| $\|1\,-\frac{1}{2}\,\frac{1}{2}\,\frac{1}{2}\,J\,I\,m_J\,m_I\rangle$ | $^2\Pi_{\frac{1}{2}}$ |
| $\|-1\,\frac{1}{2}\,-\frac{1}{2}\,\frac{1}{2}\,J\,I\,m_J\,m_I\rangle$ | $^2\Pi_{-\frac{1}{2}}$ |
| $\|0\,\frac{1}{2}\,\frac{1}{2}\,\frac{1}{2}\,J\,I\,m_J\,m_I\rangle$ | $^2\Sigma_{\frac{1}{2}}$ |
| $\|0\,-\frac{1}{2}\,-\frac{1}{2}\,\frac{1}{2}\,J\,I\,m_J\,m_I\rangle$ | $^2\Sigma_{-\frac{1}{2}}$ |

**J** and **I** on an axis fixed in space. The vector model of this coupling case is shown in Fig. 5(a). The quantum number $\Omega$ takes on the values $\Omega=\Lambda+\Sigma$, where $\Lambda=0$, $\pm1$, $\pm2$, $\cdots$ and $\Sigma=S$, $S-1$, $\cdots$ $-S$. The oxygen molecule, on the other hand, is a good Hund's case (b) molecule: **S** is only weakly coupled to the molecular axis (in oxygen the coupling is via the spin-spin interaction), and this coupling is broken almost completely by the molecular rotation. The appropriate strong-field base functions, again written in terms of good quantum numbers, are $|\Lambda\,K\,S\,J\,I\,m_J\,m_I\rangle$, where $K$ is the quantum number of $\mathbf{K}=\mathbf{L}+\mathbf{N}$; the vector model is shown by Fig. 5(b). In both these pure coupling cases, case (a) and case (b), molecular terms are labelled by particular values of $|\Lambda|$ and $S$; thus, $S=\frac{1}{2}$ gives doublet terms and these are written $^2\Sigma$ for $|\Lambda|=0$, $^2\Pi$ for $|\Lambda|=1$, and so on. Common to both cases is also a twofold $\pm\Lambda$ degeneracy of all energy levels for $|\Lambda|\neq0$.

The hydroxyl radicals OH and OD present a more complex coupling case. The very fast rotation of these light molecules, competing with the spin-orbit interaction, produces a spin coupling intermediate between case (a) and case (b), i.e., **S** is partially uncoupled from the molecular axis. To a small extent the rotation also uncouples **L** from the molecular axis, and this removes the $\pm\Lambda$ degeneracy of the case (a) or (b) energy levels. This is the "$\Lambda$-type doubling" mentioned earlier, whose effect is shown in Fig. 4 as a splitting of all the molecular energy levels into closely spaced pairs.

Wave functions that reflect the partial uncoupling of both **L** and **S** can, in principle, be constructed from either case (a) or case (b) base functions; case (a) is more convenient, however, because the theoretical analysis of **L** uncoupling for $^2\Pi$ terms has been worked out in this representation.[1,18] Linear combinations of the six case (a) functions shown in Table I are required for an adequate description of both the **L** and **S** uncoupling. The two $^2\Sigma$ functions ($\Lambda=0$) are donated by the first excited electronic term, located some $3\times10^4$ cm$^{-1}$ above the ground $^2\Pi$ term. A more exact description of the **L** uncoupling, unnecessary here, would bring in other more highly excited terms. In spectroscopic notation, the two linear combinations that correspond to a given $\Lambda$-type doublet have the form:

$$\begin{aligned}\sqrt{2}\psi_0^+&=C_1^+(\Pi_{\frac{3}{2}}+\Pi_{-\frac{3}{2}})+C_2^+(\Pi_{\frac{1}{2}}+\Pi_{-\frac{1}{2}})\\&\quad+C_3^+(\Sigma_{\frac{1}{2}}+\Sigma_{-\frac{1}{2}}),\\\sqrt{2}\psi_0^-&=C_1^-(\Pi_{\frac{3}{2}}-\Pi_{-\frac{3}{2}})+C_2^-(\Pi_{\frac{1}{2}}-\Pi_{-\frac{1}{2}})\\&\quad+C_3^-(\Sigma_{\frac{1}{2}}-\Sigma_{-\frac{1}{2}}).\end{aligned}\tag{2}$$

Each of these linear combinations has a definite symmetry with respect to reflection in a plane containing the molecular axis: $\psi_0^+$ is unchanged by such a reflection, while $\psi_0^-$ changes sign. The symmetry of the Zeeman operator (1) is such that it does not connect states of different symmetry, that is, $(\psi_0^\pm|Z|\psi_0^\mp)=0$. This means that the Zeeman effects of the two types of states will be completely independent, and furthermore that no magnetic dipole transitions of the $+\leftrightarrow-$ type can occur. The reverse holds for electric dipole transitions, where only the $+\leftrightarrow-$ type are allowed.

The amplitudes $C_\mu^\pm$, where $\mu=1, 2, 3$, are given by the secular equations:

$$\begin{aligned}&\textstyle\sum_\mu C_\mu^+(H_{k\mu}^+-\delta_{k\mu}W_0^+)=0,\\&\textstyle\sum_\mu C_\mu^-(H_{k\mu}^--\delta_{k\mu}W_0^-)=0,\quad k=1, 2, 3\end{aligned}\tag{3a}$$

together with the normalization conditions

$$\textstyle\sum_\mu|C_\mu^+|^2=\sum_\mu|C_\mu^-|^2=1.\tag{3b}$$

The $H_{k\mu}^\pm$ are the matrix elements of the combined rotational and spin-orbit interaction,[18] and the $W_0^\pm$ are the energy eigenvalues of this matrix. These energies have been calculated by Van Vleck[18] to first order in $(E_\Sigma-E_\Pi)^{-1}$, the inverse energy separation of the $\Pi$ and $\Sigma$ terms, and to second order by DST. The first order solutions are adequate here, and on substitution into (3) they yield the following amplitudes, which are correct (and normalized) to first order in $(E_\Sigma-E_\Pi)^{-1}$ $(\equiv E^{-1})$:

$$\begin{aligned}C_1^+&=\left[\frac{X\pm(2-\lambda)}{2X}\right]^{\frac{1}{2}}\left\{1\pm\frac{X\mp(2-\lambda)}{2X}\frac{(\theta+\zeta)^2-\eta^2}{EB_pX}\right.\\&\qquad\left.\pm\frac{2-\lambda}{X}\left[\frac{X\mp(2-\lambda)}{X\pm(2-\lambda)}\right]^{\frac{1}{2}}\frac{(\theta+\zeta)\eta}{EB_pX}\right\},\\C_2^+&=\mp\left[\frac{X\mp(2-\lambda)}{2X}\right]^{\frac{1}{2}}\left\{1\pm\frac{X\pm(2-\lambda)}{2X}\frac{(\theta+\zeta)^2-\eta^2}{EB_pX}\right.\\&\qquad\left.\mp\frac{2-\lambda}{X}\left[\frac{X\pm(2-\lambda)}{X\mp(2-\lambda)}\right]^{\frac{1}{2}}\frac{(\theta+\zeta)\eta}{EB_pX}\right\},\\C_3^+&=\pm\left[\frac{X\mp(2-\lambda)}{2X}\right]^{\frac{1}{2}}\frac{\theta+\zeta}{E}-\left[\frac{X\pm(2-\lambda)}{2X}\right]^{\frac{1}{2}}\frac{\eta}{E},\end{aligned}\tag{4}$$

where

$$\begin{aligned}&X\equiv+[4(J+\tfrac{1}{2})^2+\lambda(\lambda-4)]^{\frac{1}{2}},\quad\lambda\equiv A/B_p,\\&\theta\equiv(\Pi|AL_y+2BL_y|\Sigma),\\&\zeta\equiv2(J+\tfrac{1}{2})(\Pi|BL_y|\Sigma),\\&\eta\equiv2[(J+\tfrac{3}{2})(J-\tfrac{1}{2})]^{\frac{1}{2}}(\Pi|BL_y|\Sigma).\end{aligned}$$

[18] J. H. Van Vleck, Phys. Rev. **33**, 467 (1929).

The values of $C_\mu^-$ are given by relations that differ from (4) only in a reversal of the sign before $\zeta$. The parameter $\lambda$, the ratio of the spin-orbit coupling constant of the $^2\Pi$ term to its rotational constant, is a measure of the spin uncoupling. The degree of **L** uncoupling is determined jointly by the two off-diagonal matrix elements, $(\Pi|AL_y+2BL_y|\Sigma)$ and $(\Pi|BL_y|\Sigma)$, that appear in $\theta$, $\zeta$, and $\eta$. These matrix elements involve the radial dependence of the molecular wave functions, and are best evaluated from experimental data on the $\Lambda$-type doubling.

The expressions (2) and (4) are rather general, in that they yield wave functions for all the fine structure-rotational levels of any $^2\Pi$ molecular term perturbed slightly by a $^2\Sigma^+$ term.[19] The numerical value of $\lambda$ will be positive or negative according to whether the fine structure is normal or inverted; the numerical value of $E$ will be positive or negative according to whether the $^2\Sigma$ term lies above or below the $^2\Pi$ term. The ambiguous signs in (4) are to be chosen in a consistent manner throughout; the upper signs go with one level, the lower signs with another. For a pure case (a) molecule, i.e., for $|\lambda| \to \infty$, these two levels would be designated $^2\Pi_{|\Omega|}$, $J$, where $|\Omega|$ takes the values $\frac{1}{2}$ and $\frac{3}{2}$. Inspection of (2) and (4) shows that for positive $\lambda$ the upper signs would go with the $^2\Pi_{\frac{1}{2}}$, $J$, level, the lower signs with the $^2\Pi_{\frac{3}{2}}$, $J$, level. For negative $\lambda$ the connection would be reversed. In intermediate coupling this designation of levels loses much of its meaning, but it can be retained as a convenience: one may trace in imagination a given intermediate coupling level back to its ancestor level in case (a), and label it accordingly. Thus, for instance, the phrase "$^2\Pi_{\frac{3}{2}}$, $J=\frac{3}{2}$ level" will be used in the following discussion to mean "that level in intermediate coupling whose ancestor in pure case (a) is $^2\Pi_{\frac{3}{2}}$, $J=\frac{3}{2}$." Where ambiguous signs appear in following mathematical expressions, the rules of sign choice remain those described above for pure case (a); for OH and OD, upper signs refer to "$^2\Pi_{\frac{3}{2}}$, $J$, levels," lower signs refer to "$^2\Pi_{\frac{1}{2}}$, $J$, levels."

*Molecular g factors.* The angular momentum **J** is a constant of the motion for the zero-order states (2), regardless of the extent of intermediate coupling, and is space quantized in the laboratory frame of reference. The nuclear spin **I** is also space quantized in the laboratory frame. Thus if the Zeeman operator (1) can be rewritten in the form $Z=\mu_0(g_J{}^{\rm op}\mathbf{J}+g_I\mathbf{I})\cdot\mathfrak{IC}$, where $g_J{}^{\rm op}$ is a scalar operator, the linear Zeeman effect will be just

$$(\psi_0{}^\pm|Z|\psi_0{}^\pm)=\mu_0\mathfrak{IC}[(\psi_0{}^\pm|g_J{}^{\rm op}|\psi_0{}^\pm)m_J+g_Im_I] \equiv\mu_0\mathfrak{IC}(g_J{}^\pm m_J+g_Im_I), \quad (5)$$

and the theoretical problem will be reduced to that of calculating $g_J{}^\pm$, the two numerical $g$ factors of a general $\Lambda$-type doublet. This approach, parallel to that used in defining atomic $g$ factors, involves the projection of the angular momenta **L**, **S**, and **N** onto the direction of **J**. The resulting expression for the $g$-factor operator, when expanded in the molecular frame of reference, is

$$g_J{}^{\rm op}=[J(J+1)]^{-1}[(g_l-g_N)(L_xJ_x+L_yJ_y+L_zJ_z) +(g_s-g_N)(S_xJ_x+S_yJ_y+S_zJ_z)+g_N\mathbf{J}^2], \quad (6)$$

where the $z$ axis is the symmetry axis of the molecule. The matrix elements of $g_J{}^{\rm op}$ diagonal in $J$ in the case (a) representation can be constructed from the matrix elements of angular momentum given by Van Vleck. They are:

$$\begin{aligned}
&(\Lambda\Sigma\Omega JS|g_J{}^{\rm op}|\Lambda\Sigma\Omega JS)\\
&\quad=[J(J+1)]^{-1}\{(g_l\Lambda+g_s\Sigma)\Omega+g_N[J(J+1)-\Omega^2]\},\\
&(\Lambda\Sigma\Omega JS|g_J{}^{\rm op}|\Lambda\ \Sigma\pm1\ \Omega\pm1\ JS)\\
&\quad=-\tfrac{1}{2}(g_s-g_N)[J(J+1)]^{-1}[J(J+1)-\Omega(\Omega\pm1)]^{\frac{1}{2}} \times[S(S+1)-\Sigma(\Sigma\pm1)]^{\frac{1}{2}},\\
&(\Lambda\Sigma\Omega JS|g_J{}^{\rm op}|\Lambda\pm1\ \Sigma\ \Omega\pm1\ JS)\\
&\quad=-(g_l-g_N)[J(J+1)]^{-1}(\Lambda|L_y|\Lambda\pm1) \times[J(J+1)-\Omega(\Omega\pm1)]^{\frac{1}{2}}.
\end{aligned} \quad (7)$$

Using these matrix elements and the wave functions (2), one finds for the molecular $g$ factors:

$$\begin{aligned}
g_J{}^+&=g_J{}^0+(\delta g_J)_S+(\delta g_J)_N+(\delta g_J)_L{}^+,\\
g_J{}^-&=g_J{}^0+(\delta g_J)_S+(\delta g_J)_N+(\delta g_J)_L{}^-,
\end{aligned} \quad (8)$$

where

$$g_J{}^0=\frac{1}{J(J+1)}\left(\frac{3}{2}\pm\frac{2Y^2-\frac{3}{2}\lambda+3}{X}\right),$$

$$(\delta g_J)_S=\frac{g_s-2}{4J(J+1)X}[X\pm2(2-\lambda)\pm4Y^2],$$

$$(\delta g_J)_N=g_N\left[1-\frac{5X\pm4(2-\lambda)\mp4Y^2}{4J(J+1)X}\right],$$

$$(\delta g_J)_L{}^+=\pm\frac{2Y(\lambda+1)}{B_pJ(J+1)X^3}\left[(2-\lambda)\frac{(\theta+\zeta)\eta}{E}-Y\frac{(\theta+\zeta)^2-\eta^2}{E}\right]$$

$$+\frac{2(\Pi|L_y|\Sigma)}{J(J+1)X}\left\{\left[\mp Y^2+\frac{X\mp(2-\lambda)}{2}(J+\tfrac{1}{2})\right]\frac{\theta+\zeta}{E}\right.$$

$$\left.+Y\left[\mp(J+\tfrac{1}{2})+\frac{X\pm(2-\lambda)}{2}\right]\frac{\eta}{E}\right\},$$

[19] The intrinsic symmetry properties of the $^2\Sigma$ term, exclusive of electron spin, must be considered when constructing the wave functions. For perturbation by a $^2\Sigma^+$ term the linear combinations (2) are correct; for perturbation by a $^2\Sigma^-$ term the third term of $\psi_0{}^+$ should be interchanged with the third term of $\psi_0{}^-$. See reference 18 for further discussion of this point.

$$(\delta g_J)_L{}^- = \pm\frac{2Y(\lambda+1)}{B_v J(J+1)X^3}\left[(2-\lambda)\frac{(\theta-\zeta)\eta}{E}-Y\frac{(\theta-\zeta)^2-\eta^2}{E}\right]$$
$$+\frac{2(\Pi|L_y|\Sigma)}{J(J+1)X}\left\{\left[\mp Y^2-\frac{X\mp(2-\lambda)}{2}(J+\tfrac{1}{2})\right]\frac{\theta-\zeta}{E}\right.$$
$$\left.+Y\left[\pm(J+\tfrac{1}{2})+\frac{X\pm(2-\lambda)}{2\cdot}\right]\frac{\eta}{E}\right\},$$

and

$$Y\equiv[(J+\tfrac{3}{2})(J-\tfrac{1}{2})]^{\frac{1}{2}}.$$

The $g$ factors have been written as a sum of small corrections to $g_J{}^0$, the value that would be calculated from the approximate Zeeman operator $\mu_0(\mathbf{L}+2\mathbf{S})\cdot\mathcal{H}$ and wave functions that account for **S** uncoupling but not the smaller effects of **L** uncoupling. The first correction term, $(\delta g_J)_S$, proportional to $(g_s-2)$, arises from the anomalous spin magnetic moment of the electron. The second correction term, $(\delta g_J)_N$, accounts for rotation of the nuclei; in the higher rotational levels, $(\delta g_J)_N \simeq g_N$. The last term is a correction for **L** uncoupling. Since this correction stems from the interaction between electronic motion and molecular rotation, its physical interpretation is clear: $(\delta g_J)_L\mu_0$ is the extra magnetic moment contributed by electrons that participate in the end-over-end rotation of the molecule. The net effect of rotation on the molecular magnetic moment is then $(\delta g_J)_N\mu_0+(\delta g_J)_L\mu_0$, the sum of the nuclear and electronic contributions. Coming from rotating charges of opposite sign, the two contributions partially cancel each other. These rotational effects are very similar to those that produce the entire magnetic moment of $\Sigma$ states of diatomic molecules.[20]

The theoretical expressions for $(\delta g_J)_L$ are complicated by the effects of spin-uncoupling, as evidenced by the ubiquitous occurrence of $\lambda$ and $X$. Nevertheless, inspection of the signs of individual terms shows that $(\delta g_J)_L{}^+$ differs considerably from $(\delta g_J)_L{}^-$, and this leads to measurable differences between the $g$ factors $g_J{}^+$ and $g_J{}^-$.

### *1.2 Higher Order Zeeman Effects*

The linear Zeeman effect (5) calculated in the preceding section is the leading term of an expansion of the Zeeman energies in powers of $\mu_0\mathcal{H}$. For the magnetic field strengths used in this experiment, the expansion must be continued to higher order in $\mu_0\mathcal{H}$ to match in accuracy the experimental results. The quadratic term must be included for all the levels investigated, and in one case the cubic term must also be considered. These higher order Zeeman effects, which originate in the mixing of the zero-order levels by the applied magnetic field, may be calculated with the standard perturbation theory formulas listed by Condon and Shortley,[21] together with matrix elements given by Lin and Mizushima.[8] The Zeeman operator (1) and the wave functions (2), (4) are unnecessarily precise for this calculation. Instead, one may use for $Z$ the approximate form $\mu_0(\mathbf{L}+2\mathbf{S})\cdot\mathcal{H}$ and in $\psi_0{}^\pm$ one may set $C_3{}^\pm=0$ and replace the curly brackets in (4) by unity; this abridgement of the wave functions amounts to neglect of the small **L** uncoupling effects. The general form of the results of the calculation is

$$\Delta_2 W=(K_0+K_2 m_J{}^2)(\mu_0\mathcal{H})^2/hc \qquad (9)$$

for the quadratic Zeeman energies, and

$$\Delta_3 W=(K_1 m_J+K_3 m_J{}^3)(\mu_0\mathcal{H})^3/(hc)^2 \qquad (10)$$

for the cubic Zeeman energies. The $K$'s are dimensionless constants characteristic of a given zero-order molecular level. To the extent that the $\Lambda$-type doublet splittings are negligibly small in comparison with the separations between doublets, a satisfactory approximation here, these constants are the same for both members of a given $\Lambda$-type doublet. The perturbation calculation yields complicated formulas from which numerical values of $K_0$, $K_1$, $K_2$ and $K_3$ may be found. Alternatively, the $K$'s can be treated as unknown constants, to be evaluated from the observed paramagnetic resonance spectra (the constant $K_0$ cannot be so determined, since it leads to an equal shift of each magnetic sublevel). The comparison of these measured values of the constants with the calculated values serves as a further test of the molecular Zeeman theory; such a test has more than passing interest because of the results of the molecular beam experiment on oxygen, which showed a serious discrepancy between the calculated and the observed quadratic Zeeman effect.

## 2. Hyperfine Structure

The theory of magnetic dipole hfs in diatomic molecules has been developed by Frosch and Foley,[22] and the application of the theory to the hydroxyl radicals has been discussed by DST for the case where the hfs interaction is much stronger than Zeeman interactions, i.e., the weak-field case. For the interpretation of hfs effects in the paramagnetic resonance spectra, it is necessary to translate the work of DST into the strong-field representation. The electric quadrupole interaction in OD is small,[1] and may be disregarded here.

The hfs Hamiltonian of Frosch and Foley, with numerical corrections by Dousmanis,[23] is

$$H_{\rm hfs}=a\mathbf{I}\cdot\mathbf{L}+(b+c)I_zS_z+\tfrac{1}{2}b(I^+S^-+I^-S^+)$$
$$+\tfrac{1}{2}d(e^{2i\varphi}I^-S^-+e^{-2i\varphi}I^+S^+)$$
$$+e[e^{i\varphi}(S^-I_z+I^-S_z)+e^{-i\varphi}(S^+I_z+I^+S_z)], \qquad (11a)$$

[20] C. H. Townes and A. L. Schawlow, *Microwave Spectroscopy* (McGraw-Hill Book Company, Inc., New York, 1955), p. 290.

[21] E. U. Condon and G. H. Shortley, *The Theory of Atomic Spectra* (Cambridge University Press, New York, 1953), p. 34.

[22] R. A. Frosch and H. M. Foley, Phys. Rev. **88**, 1347 (1952).

[23] G. C. Dousmanis, Phys. Rev. **97**, 967 (1955).

where

$$\begin{aligned}
&I^+=I_x+iI_y, \quad I^-=I_x-iI_y,\\
&S^+=S_x+iS_y, \quad S^-=S_x-iS_y,\\
&a=2g_I\mu_0^2\langle 1/r^3\rangle_{\rm av},\\
&b=-g_I\mu_0^2\langle(3\cos^2\chi-1)/r^3\rangle_{\rm av}\\
&\qquad\qquad +(16\pi/3)g_I\mu_0^2\Psi^2(0),\\
&c=3g_I\mu_0^2\langle(3\cos^2\chi-1)/r^3\rangle_{\rm av},\\
&d=3g_I\mu_0^2\langle\sin^2\chi/r^3\rangle_{\rm av},\\
&e=3g_I\mu_0^2\langle\sin\chi\cos\chi/r^3\rangle_{\rm av}.
\end{aligned} \tag{11b}$$

The first term in $H_{\rm hfs}$ represents the interaction of the nuclear magnetic moment with the magnetic field generated by electronic orbital motion; the remaining terms represent the dipole-dipole interaction between the nuclear magnetic moment and the electron spin magnetic moment, generalized to account for a possible relativistic hfs interaction such as in characteristic of $s$ electrons in atoms. The relativistic hfs interaction is proportional to $\Psi^2(0)$, the density of unpaired electrons at the magnetic nucleus (in this case H or D), and is included in the classical dipole-dipole term by redefining the interaction constant $b$. The averages involved in the constants $a$, $b$, $c$, $d$, and $e$ are to be taken over the space coordinates of the electron responsible for the hfs interaction; $\mathbf{r}$ is the radius vector from the magnetic nucleus to the electron and $\chi$ is the angle included between $\mathbf{r}$ and the molecular axis. If more than one electron contributes to the hfs, the interaction constants will contain a term from each contributing electron.

Using the case (a) matrix elements of $H_{\rm hfs}$ calculated by Frosch and Foley, together with the zero-order wave functions (2), one finds that the first order hfs energies are, to sufficient accuracy,

$$\begin{aligned}
W_{\rm hfs}^+&=(\psi_0^+|H_{\rm hfs}|\psi_0^+)=(A_1+A_2)m_Jm_I,\\
W_{\rm hfs}^-&=(\psi_0^-|H_{\rm hfs}|\psi_0^-)=(A_1-A_2)m_Jm_I,
\end{aligned} \tag{12a}$$

where

$$\begin{aligned}
A_1=&[\pm 4J(J+1)X]^{-1}\{2a(\pm 2X+2-\lambda)\\
&+b[\pm X+4-2\lambda-4(J+\tfrac{3}{2})(J-\tfrac{1}{2})]\\
&+c(\pm X+4-2\lambda)\},\\
A_2=&\,d[\pm 4J(J+1)X]^{-1}(\pm X-2+\lambda)(J+\tfrac{1}{2}).
\end{aligned} \tag{12b}$$

The expressions for $A_1$ and $A_2$ can also be written down directly from the paper of DST, except for an incorrect sign before the term $4(J-\frac{1}{2})(J+\frac{3}{2})$ in their equivalent of $A_1$. The $A_2$ term represents the "hyperfine doubling"; its origin is in cross terms of the type $(\Pi_{\frac{3}{2}}|H_{\rm hfs}|\Pi_{-\frac{1}{2}})$ that occur in the expansion of $(\psi_0^\pm|H_{\rm hfs}|\psi_0^\pm)$. Other nonzero cross terms of the type $(\Pi|H_{\rm hfs}|\Sigma)$ also appear in the expansion, but they have been omitted from (12a). Their contribution to the hfs is comparable in magnitude with second order terms resulting from: (1) hyperfine interactions between neighboring Zeeman levels, which contribute terms of order $(W_{\rm hfs})^2/\mu_0\mathfrak{IC}$, and (2) hyperfine interactions off-diagonal in $J$, which enter through magnetic field mixing of the zero-order levels—their order of magnitude is $W_{\rm hfs}\mu_0\mathfrak{IC}/\delta$, where $\delta$ is the energy separation between a given zero-order level and the nearest neighboring level with which it is admixed by the magnetic field. Approximate calculations show that none of these three contributions to the hfs seriously exceeds the experimental uncertainty in measuring the paramagnetic resonance spectra, and all are disregarded.

### 3. Paramagnetic Resonance Spectra

*Identification.* Collecting results, one can write for the energies of a given $\Lambda$-type doublet, in a moderately intense magnetic field,

$$\begin{aligned}
W^\pm=&\bar{W}_0\pm\tfrac{1}{2}h\nu_\Lambda+(g_J^\pm m_J+g_Im_I)\mu_0\mathfrak{IC}\\
&+(K_0+K_2m_J^2)(\mu_0\mathfrak{IC})^2/hc+(K_1m_J+K_3m_J^3)\\
&\times(\mu_0\mathfrak{IC})^3(hc)^2+(A_1\pm A_2)m_Jm_I,
\end{aligned} \tag{13}$$

where $\bar{W}_0$ is the mean energy and $h\nu_\Lambda$ the energy splitting of the zero-order $\Lambda$-type doublet. By "moderately intense" is meant a field strength such that $|W_{\rm hfs}|\ll\mu_0\mathfrak{IC}\ll|\delta|$; since $|W_{\rm hfs}|\lesssim 10^{-3}$ cm$^{-1}$ and $\delta\gtrsim 50$ cm$^{-1}$ for all the levels of Fig. 4, this condition on the magnetic field strength is rather easily satisfied. There are $2(2J+1)(2I+I)$ energy sublevels contained in (13). Figure 6 shows a conventional representation of the sixteen sublevels of the ground level of OH ($^2\Pi_{\frac{3}{2}}$, $J=\frac{3}{2}$, $I=\frac{1}{2}$). Similar diagrams, differing in the number of sublevels and the size of the $\Lambda$-type doubling interval, can be drawn for the other levels of Fig. 4. Measured values of $\nu_\Lambda$, the $\Lambda$-type doubling frequency, range from the 1.7 kMc/sec of Fig. 6 to about 37 kMc/sec for the $^2\Pi_{\frac{3}{2}}$, $J=11/2$ level.

The $\Lambda$-type doubling permits paramagnetic resonance transitions of the electric dipole type, as well as the more common magnetic dipole type. The electric dipole transitions may be excited by a perpendicular (with respect to the direction of the static magnetic field) component of the microwave electric field, while the magnetic dipole transitions require a perpendicular component of the microwave magnetic field. The usual paramagnetic resonance selection rules $\Delta m_J=\pm 1$ and $\Delta m_I=0$ govern both types of transitions, but the corresponding spectra are sharply differentiated by the additional selection rules $+\leftrightarrow-$ for electric dipole transitions, and $+\leftrightarrow+$, $-\leftrightarrow-$ for magnetic dipole transitions: magnetic dipole transitions take place *in*, electric dipole transitions take place *between*, the two members of the $\Lambda$-type doublet. The complete set of paramagnetic resonance transitions in the ground level of OH is shown by arrows in Fig. 6—solid arrows for the twelve electric dipole transitions and dashed arrows for the twelve magnetic dipole transitions [in general, there are $4J(2I+1)$ transitions of each

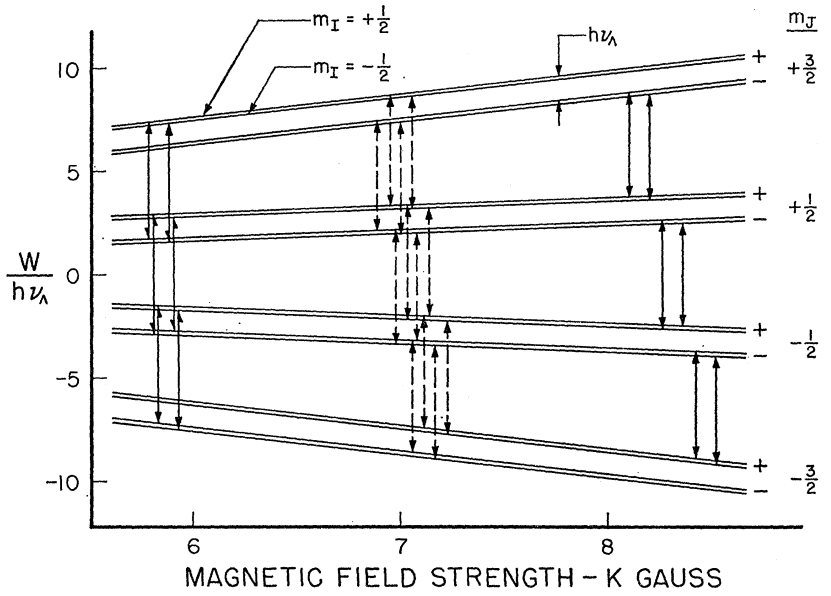


FIG. 6. Energy sublevels and paramagnetic resonance transitions for $O^{16}H$, $^2\Pi_{\frac{3}{2}}$, $J=\frac{3}{2}$. Magnetic dipole transitions (not observed in this experiment) are indicated by dashed arrows, electric dipole transitions by solid arrows. The small magnetic field separations within the three groups of transitions are exaggerated for clarity.

type]. These arrows are all drawn to approximately the same length, to correspond with a constant observing frequency of 9.5 kMc/sec. The abscissas of the arrows thus give a crude prediction of the paramagnetic resonance spectrum. Notice that although the magnetic dipole transitions cluster about a magnetic field strength that corresponds to the molecular $g$ factor, the electric dipole transitions are displaced in two groups far to either side. The separation of these high- and low-field groups is a measure of the $\Lambda$-type doubling interval. On comparing Fig. 6 with Fig. 1, one sees the reason for identifying one group of absorption lines in Fig. 1 as the $^2\Pi_{\frac{3}{2}}$, $J=\frac{3}{2}$, $(m_J)^+ \leftrightarrow (m_J-1)^-$ electric dipole spectrum and another group as the $^2\Pi_{\frac{3}{2}}$, $J=\frac{3}{2}$, $(m_J)^- \leftrightarrow (m_J-1)^+$ electric dipole spectrum. The other two groups of absorption lines in Fig. 1 are identified as the $^2\Pi_{\frac{3}{2}}$, $J=\frac{5}{2}$, $(m_J)^+ \leftrightarrow (m_J-1)^-$ electric dipole spectrum and the $^2\Pi_{\frac{3}{2}}$, $J=\frac{7}{2}$, $(m_J)^- \leftrightarrow (m_J-1)^+$ electric dipole spectrum in an exactly similar way. For these latter two molecular levels the $\Lambda$-type doubling intervals are so large that only one group of electric dipole transitions can be observed at $X$-band frequencies and magnetic field strengths below 11 kgauss. The identification of the absorption spectrum in Fig. 2 as the $^2\Pi_{\frac{3}{2}}$, $J=\frac{3}{2}$ electric dipole spectrum of OD is clear from its similarity with the corresponding spectrum of OH. The $\Lambda$-type doubling interval is smaller, but this is to be expected for a heavier, more slowly rotating molecule. The total number of lines, eighteen, is correct for a nuclear spin of unity, corresponding to the deuteron of OD.

The spectra of Figs. 1 and 2 include all of the $^2\Pi_{\frac{3}{2}}$ electric dipole spectra that are predicted to fall within the range of our instrument. Also predicted, but not observed, are spectra of two OH $^2\Pi_{\frac{1}{2}}$ levels ($J=\frac{3}{2}$ and $J=\frac{5}{2}$), as well as the magnetic dipole $^2\Pi_{\frac{3}{2}}$, $J=\frac{3}{2}$ spectrum for both OH and OD. Because of the low expected intensities of these spectra, the failure to observe them is not surprising. The more intense of the two $^2\Pi_{\frac{3}{2}}$ spectra, originating in the $J=\frac{3}{2}$ level, should give absorption signals over 120 times weaker than those observed for the corresponding $^2\Pi_{\frac{3}{2}}$ spectrum: the electric dipole transition probability is nearly nine times smaller,[1] the level population is two times smaller, and the $g$ factor seven times smaller. The effect of the smaller $g$ factor is felt not as a reduction of the over-all intensity of the spectrum, but rather as an inversely proportionate increase of the width, measured in magnetic field units, of each absorption line. The magnetic dipole spectra, on the other hand, should be reduced in intensity approximately by the ratio $(\mu_m)^2/(\mu_e)^2$, where $\mu_m$ is the molecular magnetic moment and $\mu_e$ the electric dipole moment; for a magnetic moment of one Bohr magneton and an electric moment of 1.5 Debye units,[24] this ratio is $5\times10^{-5}$. Implicit in these intensity comparisons is the assumption that the microwave field intensities are equal in each case, and thus that the transition probabilities are proportional to the squares of the dipole moments. In principle one can equalize the transition probabilities by adjusting the microwave power level, and thereby increase the strength of the weaker absorption signals. However, a large part of this advantage is lost if, as in our apparatus, the spectrometer noise level increases rapidly with microwave power level. For the OH magnetic dipole spectrum, whose line positions could be calculated accurately from the observed electric dipole spectra, several slow searches were made, using a high microwave power level and a long output time constant, over a range of magnetic

[24] R. P. Madden and W. S. Benedict, J. Chem. Phys. 23, 408 (1955).

field strengths that spanned the predicted spectrum. Under these conditions the magnetic dipole spectrum of atomic hydrogen, also produced in the water vapor discharge, was approximately 3000 times above noise, yet no magnetic dipole absorption by OH was detectable.

*Analysis.* The electric dipole transition energies are given by the energy differences $h\nu=W^+(m_J,m_I)-W^-(m_J-1, m_I)$ or $h\nu=W^-(m_J,m_I)-W^+(m_J-1, m_I)$. These are, from (13),

$$\begin{aligned}h\nu=&-h\nu_\Lambda+g_J{}^+\mu_0\mathfrak{H}\mathcal{C}+(g_J{}^--g_J{}^+)m_J\mu_0\mathfrak{H}\mathcal{C}\\&+K_2(2m_J-1)(\mu_0\mathfrak{H}\mathcal{C})^2/hc\\&+[K_1-K_3-3K_3m_J(m_J-1)](\mu_0\mathfrak{H}\mathcal{C})^3/(hc)^2\\&+[A_1-(2m_J-1)A_2]m_I,\end{aligned}\quad(14)$$

and

$$\begin{aligned}h\nu=&+h\nu_\Lambda+g_J{}^-\mu_0\mathfrak{H}\mathcal{C}-(g_J{}^--g_J{}^+)m_J\mu_0\mathfrak{H}\mathcal{C}\\&+K_2(2m_J-1)(\mu_0\mathfrak{H}\mathcal{C})^2/hc\\&+[K_1-K_3-3K_3m_J(m_J-1)](\mu_0\mathfrak{H}\mathcal{C})^3/(hc)^2\\&+[A_1+(2m_J-1)A_2]m_I,\end{aligned}\quad(15)$$

where $m_I$ may take on any of the values $I, I-1, \cdots -I$, but $m_J$ is limited to the values $J, J-1, \cdots -(J-1)$. The spectra are observed by varying the magnetic field strength to bring successive transitions into resonance at the constant microwave frequency $\nu$. For $\nu>\nu_\Lambda$, the high-field transitions are given by (14), the low-field transitions by (15). If $\nu_\Lambda$ is appreciably larger than $\nu$, (15) cannot be satisfied at any field strength, and the corresponding spectrum will not appear. The third term in each of these resonance equations is a rather interesting manifestation of the **L** uncoupling phenomenon. This term displaces the spectral lines in much the same way as does the following term, which arises from the quadratic Zeeman effect. Since the two terms subtract in one resonance equation and add in the other, the resultant line splittings in the low-field spectrum may differ considerably from those in the high-field spectrum. The two $^2\Pi_{\frac{3}{2}}$, $J=\frac{3}{2}$ spectra of OH in Fig. 1 give a striking visual demonstration of this effect. In the low-field spectrum the **L** uncoupling effect opposes the quadratic Zeeman effect and condenses the spectrum to three nearly superposed hfs doublets; in the high-field spectrum the reverse occurs and the line splittings are enhanced. The same effect appears, although not as strongly, in the OD spectrum of Fig. 2. In the remaining spectra of Fig. 1, the relative contributions of **L** uncoupling and quadratic Zeeman effects to the line splittings are less easy to assess, since one of the two electric dipole groups is missing in each case. Nevertheless, the two effects can be distinguished experimentally by their different dependence on magnetic field strength: comparisons of spectra recorded at different microwave frequencies show that **L** uncoupling contributes roughly 90% of the line splittings in both the $J=\frac{5}{2}$ and $J=\frac{7}{2}$ spectra. These observations on the magnetic field dependence of the line splittings also served to indicate the correct assignment of $m_J$ values to individual lines. Because the hfs splittings showed no observable field dependence, an element of ambiguity remained in the experimental assignment of $m_I$ values; this ambiguity limits the analysis only to the extent that the sign of the hfs constant $A_1$ cannot be determined from the experiment alone. The specific assignment of $m_I$ values in Fig. 1 and Fig. 2 is based on the discussion of Sec. IV.

For numerical analysis of the spectra, (14) and (15) were rewritten by inserting the nuclear magnetic resonance relation $h\nu_I=g_I\mu_0\mathfrak{H}\mathcal{C}$. Values used for the nuclear $g$ factors were $g_I(H^1)=-2/(657.469\pm0.009)^3$ and $g_I(Li^7)=(0.388636\pm0.000008)g_I(H^1)$.[25] To the desired accuracy, corrections for electronic shielding and bulk diamagnetism of the nuclear resonance sample are negligible, and were not made. On substituting values of $\nu_I$ measured at the center of each absorption line, together with the measured microwave frequency $\nu$, one gets a set of simultaneous linear equations, one equation for each line of the spectrum, which may be solved for the desired molecular constants. These constants include the $\Lambda$-type doubling frequency $\nu_\Lambda$, the molecular $g$ factors $g_J{}^+$ and $g_J{}^-$, the hfs constants $A_1$ and $A_2$, and the coefficient of the quadratic Zeeman effect, $K_2$. The cubic Zeeman effect was found to be too small to measure except in the $J=\frac{7}{2}$ spectrum, where it shifted the line positions by not more than one linewidth. The experimental results are listed in Table II. The results for a given molecular level are consistent, within experimental error, with the positions of all the lines of the corresponding spectrum, measured at two or more different microwave frequencies within the range 8.8–9.7 kMc/sec. For the $J=\frac{3}{2}$ spectra of both OH and OD, accurate values of all the constants could be found from the complete spectrum observed at a single microwave frequency; observations at other frequencies were then used to check the original results. For the incomplete $J=\frac{5}{2}$ and $J=\frac{7}{2}$ spectra, the constants were determined by combining the measurements made at two well separated microwave frequencies; these values were then checked against the spectrum recorded at an intermediate frequency. The accuracy of constants determined in this way can be rather good if the $\Lambda$-type doubling frequency is fairly close to the frequency band of the klystron, for then a small change in klystron tuning will shift the paramagnetic resonance spectrum by a disproportionately large amount. In our case a 6% change in klystron frequency led to a 20% magnetic field shift of both the $J=\frac{5}{2}$ and $J=\frac{7}{2}$ spectra, and this allowed a fairly accurate determination of the $g$ factors and $\Lambda$-type doubling frequencies for both levels. Better $g$ factors can be found for the $J=\frac{7}{2}$ level by combining the precise value of $\nu_\Lambda$ measured by DST with the data of the present experiment; these are the values actually

[25] H. E. Walchli, Oak Ridge National Laboratory Report ORNL-1469, 1953, and Suppl. No. 2, 1955 (unpublished).

TABLE II. Experimental results. Molecular $g$ factors, $\Lambda$-type doubling frequencies, coefficients of higher order Zeeman effects, and hfs coupling constants derived from the OH and OD paramagnetic resonance spectra.

| $^2\Pi_{\frac{3}{2}}$ level | $g_J^+$ | $g_J^-$ | $\nu_\Lambda$ (Mc/sec) | $K_2$ | $K_1$ | $K_3$ | $\lvert A_1\rvert$ (Mc/sec) | $\lvert A_2\rvert$ (Mc/sec) |
|---|---|---|---|---|---|---|---|---|
| $O^{16}H$ $J=\frac{3}{2}$ | 0.93493±0.00003 | 0.93622±0.00003 | 1666.34±0.10 | (3.13±0.03)×10$^{-3}$ | | | 27.01±0.05 | 0.51±0.05 |
| $J=\frac{5}{2}$ | 0.48435±0.00015 | 0.48623±0.00015 | 6033.5 ±1.0 | (0.3 ±0.1 )×10$^{-3}$ | | | 5.39±0.05 | 0.68±0.05 |
| $J=\frac{7}{2}$ | 0.32454±0.00004[a] | 0.32668±0.00004[a] | 13437.8 ±2.0 | (0.40±0.03)×10$^{-3}$ | (4±1)×10$^{-4}$ | −(3±1)×10$^{-5}$ | 1.00±0.05 | 0.87±0.05 |
| $O^{16}D$ $J=\frac{3}{2}$ | 0.88920±0.00003 | 0.88971±0.00003 | 310.12±0.08 | (3.78±0.02)×10$^{-3}$ | | | 4.84±0.03 | 0.03±0.03 |

[a] Calculated from the observed $^2\Pi_{\frac{3}{2}}$, $J=7/2$ spectrum, using the value $\nu_\Lambda=(13438.41\pm0.05)$ Mc/sec given in reference 1.

TABLE III. Values of $(\Pi|L_y|\Sigma)$ calculated from the observed $g$-factor differences.

| $^2\Pi_{\frac{3}{2}}$ level | $(g_J^- - g_J^+)_{\text{exp}}$ | $(\Pi\|L_y\|\Sigma)$ |
|---|---|---|
| $O^{16}H$ $J=\frac{3}{2}$ | 0.00129±0.00002 | 0.67±0.02 |
| $J=\frac{5}{2}$ | 0.00188±0.00008 | 0.68±0.04 |
| $J=\frac{7}{2}$ | 0.00214±0.00002 | 0.66±0.01 |
| $O^{16}D$ $J=\frac{3}{2}$ | 0.00051±0.00002 | 0.68±0.06 |

shown in Table II for $J=\frac{7}{2}$. The hfs coupling constants are calculated from the small hfs splittings within each group of absorption lines, and hence all the hfs constants, including those of the $J=\frac{5}{2}$ and $J=\frac{7}{2}$ levels, have about the same absolute uncertainty. The listed values of $A_1$ and $A_2$ are the mean results of several measurements, together with their statistical standard errors. The uncertainties quoted with the values of $\nu_\Lambda$ and $g_J$ are based partly on estimated errors in measuring the absolute strength of the magnetic field. Arising primarily from imperfect knowledge of the small field differential between the position of the magnetometer probe and the microwave cavity, these errors are unimportant in measurements of the small field increments associated with the hfs.

Two of the $\Lambda$-type doubling frequencies given in Table II, those for the $J=\frac{3}{2}$ and $J=\frac{7}{2}$ levels of OH, have also been measured in the zero-field absorption experiments[1,2]; at these two points of comparison there is satisfactory agreement, well within the experimental uncertainties, between the results obtained by the two different experimental methods.

## IV. EXPERIMENT VERSUS THEORY

### 1. Zeeman Effect

In order to calculate theoretical $g$ factors from (8), one must have numerical values of the spin-uncoupling parameter $\lambda$, the $\mathbf{L}$ uncoupling parameters $\theta$, $\zeta$, and $\eta$, and the molecular matrix element $(\Pi|L_y|\Sigma)$. The microwave absorption experiment of DST provides a direct measurement of $\lambda$, and values of $\theta$, $\zeta$, and $\eta$ can be deduced from their measured quantities $\alpha_p$ and $\beta_p$. It remains to determine $(\Pi|L_y|\Sigma)$.

Without accurate electronic wave functions, only a crude value of $(\Pi|L_y|\Sigma)$ can be calculated from theory. Under the rather drastic assumption that $\mathbf{L}^2$ is a constant of the motion (the "pure precession hypothesis"), with $L=1$, the matrix element would have the value $\sqrt{2}/2$. The results of DST indicate that this is a considerable overestimate of the true value. Fortunately, $(\Pi|L_y|\Sigma)$ enters strongly into the theoretical $g$-factor differences

$$g_J^+ - g_J^- = (\delta g_J)_L^+ - (\delta g_J)_L^-, \tag{16}$$

and thus it can be determined from a part of the $g$-factor data—the observed $g$-factor differences. Table III lists these differences and the values of $(\Pi|L_y|\Sigma)$ derived therefrom. The consistency of the four values

TABLE IV. Theoretical $g$ factors and their comparison with experiment.

| $^2\Pi_{\frac{3}{2}}$ level | $g_J^0$ | $(\delta g_J)_s$ | $(\delta g_J)_N$ | $\frac{1}{2}[(\delta g_J)_L^+ + (\delta g_J)_L^-]$ | $(\bar{g}_J)_{\text{th}}$ | $(g_J)_{\text{th}} - (\bar{g}_J)_{\text{exp}}$[a] |
|---|---|---|---|---|---|---|
| $O^{16}H$ $J=\frac{3}{2}$ | 0.93461±0.00017 | 0.00063 | −0.00026 | 0.00126±0.00002 | 0.93624±0.00019 | 0.00067±0.00022 |
| $J=\frac{5}{2}$ | 0.48460±0.00012 | 0.00037 | −0.00046 | 0.00135±0.00002 | 0.48586±0.00014 | 0.00057±0.00029 |
| $J=\frac{7}{2}$ | 0.32482±0.00009 | 0.00027 | −0.00052 | 0.00133±0.00002 | 0.32590±0.00011 | 0.00028±0.00015 |
| $O^{16}D$ $J=\frac{3}{2}$ | 0.88888±0.00015 | 0.00057 | −0.00012 | 0.00083±0.00001 | 0.89016±0.00016 | 0.00071±0.00019 |

[a] Uncertainties given here are the sums of all uncertainties experimental in origin. In addition to errors in the measurements of $(\bar{g}_J)_{\text{exp}}$, these include experimental errors in values of $\lambda$ and $(\Pi|L_y|\Sigma)$ used in calculating the theoretical $g$ factors.

is strong evidence for the correctness of the **L** uncoupling theory, and also shows that the electronic wave functions of OH and OD are, as might be expected, essentially the same.

From Table III we take the value of $(\Pi|L_J|\Sigma)$ to be 0.67±0.01 (as compared to the pure precession value 0.707). Using this, and the values of $\lambda$, $\alpha_p$ and $\beta_p$ measured by DST, the theoretical $g$ factors listed in Table IV are calculated from (8). Since half the experimental $g$-factor data has been used already to determine $(\Pi|L_y|\Sigma)$, only the four mean $g$ factors, $\bar{g}_J=(g_J^+ + g_J^-)/2$, are given. The major source of error in these theoretical $g$ factors is the experimental uncertainty in the values of $\lambda$ used to calculate $g_J^0$. The discrepancy between theory and experiment, given by the last column of Table IV, is well outside the combined theoretical and experimental errors.

Table V contains theoretical values of the Λ-type doubling frequencies and coefficients of the higher order Zeeman effects. The Λ-type doubling frequencies are calculated from the formulas of DST, including centrifugal distortion effects, and agree fairly well, probably within theoretical error, with the measured values. The theoretical values of the Zeeman coefficients $K_2$, $K_1$, and $K_3$, calculated by the method described in Sec. III, agree with the experimental values in Table II.

## 2. Hyperfine Structure

On substituting the three values of $A_1$ measured in OH into (12b), one obtains three equations linear in the three hfs constants $a$, $b$, and $c$. Unfortunately, these equations are not sufficient to determine all three constants accurately: although the equations are independent in the physical sense of arising from three different rotational energy levels, they are arithmetically independent only to the extent (in this case small) that the vector coupling scheme differs for the three levels. This difficulty is alleviated if one assumes that the same electrons are responsible for both the orbital and spin contributions to the hfs, for then, as is apparent from the definitions of $a$, $c$, and $d$, one has the further relation $c=3(a-d)$.

The value of $d$ to be inserted in this relation may be found directly from the observed hyperfine doubling: from (12b) and the values of $|A_2|$ in Table II, it is $d(\text{OH})=56\pm7$ Mc/sec. Hyperfine doubling effects were larger in the experiment of DST, and allowed a more accurate determination of $d$. Using their value, $d(\text{OH})=(57.0\pm1.5)$ Mc/sec, the remaining hfs constants are found to be[25a]

$$a(\text{OH})= 48.7\pm0.5 \text{ Mc/sec},$$
$$b(\text{OH})=113.6\pm0.6 \text{ Mc/sec},$$
$$c(\text{OH})= -25\pm5 \text{ Mc/sec}.$$

The relativistic hfs contribution, given by $b+c/3$, is 105±3 Mc/sec. The values of $a$ and $c$ above depend rather strongly on the validity of the assumption $c=3(a-d)$, and the quoted errors arise from the uncertainty in the value of $d$; the value of $b$, however, is essentially independent of this assumption, and here the quoted error is of experimental origin. The consistency of these values with all the available experimental data, including a measurement by DST of the hfs in the $J=9/2$ level of OH, is shown in Table VI. With the exception of the $J=9/2$ level, where the discrepancy is twice the experimental error, the numerical consistency of the calculated and measured values of $A_1$ is excellent. The comparison for OD shows again the practical identity of the electronic wave functions in OH and OD. Notice that the calculated values of $A_1$, in contrast to the measured values, are complete with sign; these signs have been used to assign $m_I$ values to the spectra of Figs. 1 and 2.

From the definition of the hfs constants $a$, $b$, and $c$, and from the numerical values above, the following

TABLE V. Theoretical values of the Λ-type doubling intervals and the Zeeman coefficients.

| $^2\Pi_{\frac{3}{2}}$ level | $\nu_\Lambda$ (Mc/sec) | $K_2$ | $K_1$ | $K_3$ |
|---|---|---|---|---|
| $O^{16}H$ $J=\frac{3}{2}$ | 1665.5[a] | $3.16\times10^{-3}$ | | |
| $J=\frac{5}{2}$ | 6022.8 | $0.23\times10^{-3}$ | | |
| $J=\frac{7}{2}$ | 13431.8[b] | $0.37\times10^{-3}$ | $4.2\times10^{-4}$ | $-3.2\times10^{-5}$ |
| $O^{16}D$ $J=\frac{3}{2}$ | 308.7 | $3.77\times10^{-3}$ | | |

[a] Taken from reference 2. [b] Taken from reference 1.

[25a] *Note added in proof.* Recent observations of $^2\Pi_{\frac{3}{2}}$ spectra show that the assumption $c=3(a-d)$ is not at all valid for OH, and that these hfs constants are therefore incorrect. A preliminary analysis of the combined $^2\Pi_{\frac{3}{2}}$ and $^2\Pi_{\frac{1}{2}}$ hfs data yields the new values $a(\text{OH})=85.6$ Mc/sec, $b(\text{OH})=117.4$ Mc/sec, and $c(\text{OH})=-103.0$ Mc/sec. This change does not alter the calculated values of $A_1$ in Table VI, but it does alter drastically the derived values of $\langle 1/r^3\rangle_{\text{av}}$ and $\langle(3\cos^2\chi-1)/r^3\rangle_{\text{av}}$, and, to a smaller extent, $\Psi^2(0)$. A forthcoming paper will describe the $^2\Pi_{\frac{1}{2}}$ measurements in detail.

TABLE VI. Magnetic hyperfine structure coupling constants calculated from Eq. (12b) of the text, using the values $a(\mathrm{OH})=48.7$ Mc/sec, $b(\mathrm{OH})=113.6$ Mc/sec, $c(\mathrm{OH})=-25$ Mc/sec. All entries in Mc/sec.

| $^2\Pi_{\frac{3}{2}}$ level | $(A_1)_{\mathrm{calc}}$ | $\lvert A_1\rvert_{\mathrm{calc}}-\lvert A_1\rvert_{\mathrm{exp}}$ |
|---|---|---|
| OH $J=3/2$ | 27.03 | +0.02 |
| $J=5/2$ | 5.39 | 0.00 |
| $J=7/2$ | −0.99 | −0.01 |
| $J=9/2$ | −3.29 | +0.16[a] |
| OD $J=3/2$ | 4.80[b] | −0.04 |

[a] In reference 1 the hfs interval $\Delta\nu_s=31.3\pm0.8$ Mc/sec measured in the $J=9/2$ level is equal to $(2J+1)\lvert A_1\rvert$ in the present notation; i.e., from reference 1, $\lvert A_1\rvert=3.13\pm0.08$ Mc/sec for $J=9/2$.
[b] Calculated from the relation $a(\mathrm{OD})=[g_I(\mathrm{D})/g_I(\mathrm{H})]a(\mathrm{OH})$ and corresponding relations for $b(\mathrm{OD})$ and $c(\mathrm{OD})$.

molecular constants for OH are derived:

$$\langle 1/r^3\rangle_{\mathrm{av}}=(0.616\pm0.006)\times10^{24}\ \mathrm{cm}^{-3},$$
$$\langle(3\cos^2\chi-1)/r^3\rangle_{\mathrm{av}}=-(0.21\pm0.04)\times10^{24}\ \mathrm{cm}^{-3},$$
$$\Psi^2(0)=(0.184\pm0.004)\times10^{24}\ \mathrm{cm}^{-3}.$$

To these may be added the result

$$\langle(\sin^2\chi)/r^3\rangle_{\mathrm{av}}=(0.490\pm0.009)\times10^{24}\ \mathrm{cm}^{-3}$$

derived by DST from their measured value of $d$. These constants give a rather complete description of the unpaired electron distribution about the hydrogen nucleus. In view of the excellent consistency of the OH and OD hfs measurements, the same constants may also be considered to apply to OD. This is further supported by the essential identity of $\langle\sin^2\chi/r^3\rangle_{\mathrm{av}}$ in OH and OD, as observed by DST.

In the ground electronic configuration of OH,

$$(1s\sigma)^2(2s\sigma)^2(2p\sigma)^2(2p\pi^+)^2 2p\pi^-, \qquad (17)$$

the hyperfine interaction would involve only electrons in the $\pi^{\pm}$ orbitals. These orbitals are represented in the LCAO (linear combination of atomic orbitals) scheme by $2p^{\pm}$ one-electron wave functions of atomic oxygen. Aside from their dependence on azimuthal angle the two functions are identical; this is the theoretical basis for the assumption $c=3(a-d)$. This LCAO representation of the molecular wave function is moderately successful in predicting the gross electronic energies of OH,[26] and also accounts in a rough way for the observed hyperfine structure: using a Slater-type $2p$ oxygen orbital[27] and an internuclear distance of 0.9706 A,[16] we calculate $\langle 1/r^3\rangle_{\mathrm{av}}=1.1\times10^{24}$ $\mathrm{cm}^{-3}$ and $\langle\sin^2\chi/r^3\rangle_{\mathrm{av}}=0.40\times10^{24}$ $\mathrm{cm}^{-3}$. The value of $\Psi^2(0)$ predicted by this wave function is, however, identically zero. More accurate LCAO wave functions have been constructed by superposing excited configurations, containing unpaired $\sigma$ electrons, on the ground configuration (17), and by introducing a semi-empirical correlation correction, adjusted to give the correct energies of the separated atoms.[26] The unpaired $\sigma$ electrons of the excited configurations give a nonvanishing value of $\Psi^2(0)$ at the hydrogen nucleus, but the predicted relativistic hfs constant is only 7.5 Mc/sec, as compared to the observed 105 Mc/sec.

## V. DISCUSSION

The theoretical $g$ factors of Table IV all differ from the measured values by about 0.1%, many times the experimental uncertainty. Obviously there must be rather serious defects in either the Zeeman operator (1) or in the angular wave functions (2), (4), or perhaps in both; we examine these in turn.

The Zeeman operator is known to be deficient only through its disregard of relativistic effects. In diatomic molecules, as in atoms, relativistic corrections may enter in two ways: through a velocity dependence of the electron magnetic moment and through small changes, induced by the external magnetic field, in the normal velocity-dependent interactions (spin-orbit, for example) of electrons. The explicit form of these corrections for the central field case has been derived rigorously from the Dirac-Breit equation.[3] In numerical calculations for light atoms the first effect, the relativistic alteration of the electron magnetic moment, has been found to dominate; the remaining corrections are smaller and tend to cancel each other. In the absence of a relativistic quantum theory of the two-center problem, no such accurate calculation can be made for diatomic molecules. However, the relativistic alteration of the electron moment can be estimated from classical theory, simply by including the velocity dependence of the electron mass. The resulting expression for the electron magnetic moment is $\mu_0(g_l\mathbf{l}+g_s\mathbf{s})\times(1-T/mc^2)$, where $T$ is the kinetic energy of the electron; the rigorous treatment of the central field case gives the same result. For the predominant $(\pi)^3$ electron configuration of OH and OD, the relativistic correction to the Zeeman operator becomes

$$-\mu_0(\langle T\rangle/mc^2)(\mathbf{L}+2\mathbf{S})\cdot\mathfrak{H},$$

where $\langle T\rangle$ is now the mean kinetic energy of a single $\pi$ electron. The corresponding $g$-factor correction is $-g_J{}^0\langle T\rangle/mc^2$. A glance at the last column of Table IV shows that this is the sort of correction required to bring the theoretical $g$ factors into line with experiment, provided that $\langle T\rangle/mc^2$ is approximately $1\times10^{-3}$. However, this value would be unreasonably large: the $\pi$ orbitals of the hydroxyl radical are represented rather well by the $2p$ orbitals of the oxygen atom, for which[28] $\langle T\rangle/mc^2=1.3\times10^{-4}$. It seems clear that relativistic corrections can account for only a small fraction of the discrepancy between the theoretical and measured $g$ factors.

Further errors in the Zeeman operator may arise from the use of incorrect numerical values for the electron $g$ factors $g_l$ and $g_s$, and the nuclear rotational

[26] M. Krauss and J. F. Wehner, J. Chem. Phys. **29**, 1287 (1958).
[27] R. G. Breene, Jr., Phys. Rev. **111**, 1111 (1958).
[28] A. Abragam and J. H. Van Vleck, Phys. Rev. **92**, 1448 (1953).

TABLE VII. Theoretical OH $g$ factors calculated with $\lambda=-7.500\pm0.005$ and including estimated relativistic corrections.

| $^2\Pi_{\frac{3}{2}}$ level | $g_J{}^0$ | Sum of corrections from Table IV | $-g_J{}^0\langle T\rangle/mc^2$ | $(\bar{g}_J)_{\text{th}}$ | $(\bar{g}_J)_{\text{th}}-(\bar{g}_J)_{\text{exp}}$ [a] |
|---|---|---|---|---|---|
| $O^{16}H$ $J=\frac{3}{2}$ | 0.93406±0.00005 | 0.00163±0.00002 | −0.00012 | 0.93557±0.00007 | 0 |
| $J=\frac{5}{2}$ | 0.48415±0.00004 | 0.00126±0.00002 | −0.00006 | 0.48535±0.00006 | 0.00006±0.00021 |
| $J=\frac{7}{2}$ | 0.32444±0.00003 | 0.00108±0.00002 | −0.00004 | 0.32548±0.00005 | −0.00014±0.00008 |

[a] Uncertainties estimated as in Table IV.

$g$ factor $g_N$. The value $g_l=1$, for instance, is strictly correct only for a free electron; the effective orbital $g$ factor of a molecular electron may differ slightly from unity because of relative nuclear motion. This effect has been calculated for atomic oxygen,[28] and the orbital $g$ factor was found to be $g_l=1+0.11\,m/M$, where $M$ is the mass of the oxygen nucleus. A correction of similar size (or even an order of magnitude larger) for the hydroxyl radicals would affect the theoretical $g$ factors to a completely negligible extent. The nuclear rotational $g$ factor can also be ruled out as the source of the 0.1% discrepancy: the nuclear rotation correction to the molecular $g$ factors, $(\delta g_J)_N$ in Table IV, is small and approximately the same for each rotational level. Thus $g_N$ would have to be larger by a wholly unlikely factor of two or more to account for any one of the four measured $g$ factors, and only one of the four could be so accounted for by a single new value of $g_N$. The remaining question, then, is whether it is correct to use the free-electron value of $g_s$ in computing the molecular Zeeman effect. Certainly there are compelling reasons for doing so: the many measurements of atomic $g$ factors and the measurements of the molecular oxygen and nitric oxide $g$ factors all indicate that, in either the atomic or molecular environment, the anomalous part of the electron spin moment couples to a magnetic field in the same way that the predominant Dirac part of the moment does. Nevertheless, it is interesting to observe that the theoretical $g$-factor corrections for the anomalous part of the spin moment, tabulated as $(\delta g_J)_s$ in Table IV, are numerically quite similar to the discrepancies $(\bar{g}_J)_{\text{th}}-(\bar{g}_J)_{\text{exp}}$ given in the last column.

It is clear then, that if there were no reasonable doubt in the quality of the wave functions used in the $g$-factor calculations, the results of this experiment would constitute negative evidence for an anomalous electron spin moment in the hydroxyl radicals. Regarded as a measurement of the spin $g$ factor, the experiment would yield the result $g_s(\text{OH})=g_s(\text{OD})=2.0000\pm0.0002$, where the uncertainty has been chosen large enough to account for poor knowledge of the relativistic corrections. This value is of course precisely the spin $g$ factor of a theoretical Dirac electron. To understand this result one would have to assign to the anomalous part of the spin moment special properties not shared by the Dirac part of the spin moment—properties that are displayed in the hydroxyl radicals but not in molecular oxygen and nitric oxide nor in paramagnetic atoms. Clearly, this point of view would be tenable only with a great deal more supporting evidence than is now available. We turn to an examination of the wave functions.

There can be little doubt that the form of the angular wave functions (2) is correct, nor that the amplitudes (4) are correct, to sufficient accuracy, as written. The one point where serious error can enter is in the use of an incorrect numerical value for $\lambda$, the spin uncoupling parameter. Errors in the $\mathbf{L}$ uncoupling parameters should be of no practical importance, since these parameters affect only the correction terms $(\delta g_J)_L{}^{\pm}$; although these corrections are fairly large, their accuracy has been verified adequately by the measured $g$ factor differences.[28a] The precise value of $\lambda$ is important only in the calculation of $g_J{}^0$, and even $g_J{}^0$ is not very sensitive to $\lambda$: a 0.1% change in the theoretical $g$ factors would require almost a 1% change in the experimental value of $\lambda$ quoted by DST; this is far outside their experimental uncertainty. Nevertheless, it is significant that a single new value of $\lambda$ can found that brings all three of the theoretical OH $g$ factors into much better agreement with experiment. Table VII illustrates this improved consistency when $\lambda$ is taken to have the value $-7.500\pm0.005$, instead of $-7.444\pm0.017$ as given by DST. This new value was calculated from the measured $g$ factor of the $J=\frac{3}{2}$ level, after subtracting the theoretical corrections listed in Table IV and, in addition, the relativistic correction discussed above, with $\langle T\rangle/mc^2=1.3\times10^{-4}$. If one adjusts the theoretical OD $g$ factor of Table IV in the same way to secure agreement with experiment, the new value of $\lambda$(OD) turns out to be $-14.08\pm0.01$, as compared to the value $-13.954\pm0.032$ given by DST.

Accordingly, if the quantum electrodynamic correction to the theoretical $g$ factors is taken to be correct, there is a serious discrepancy between hydroxyl radical functions derived from the measured Zeeman effect and those derived from the measured $\Lambda$-type doubling. This is particularly disturbing because of the similarity of the two experiments, both in experimental technique and in the transitions and molecular levels involved. However, this interpretation appears to draw support from earlier measurements on the ultraviolet emission

[28a] *Note added in proof.* The recent observations of $^2\Pi_{\frac{1}{2}}$ spectra also show that the absolute values of the $g$ factors, although not the $g$-factor differences, are perturbed slightly by highly excited molecular terms disregarded in Sec. III. By restricting attention to a single excited $\Sigma$ term we fail to account completely for the component of $\mathbf{L}$ in the direction of $\mathbf{N}$. A semi-empirical correction to the $g$-factor theory removes all discrepancy with experiment provided the new value $\lambda=-7.504\pm0.003$ is used for the spin uncoupling parameter.

spectra of the OH and OD radicals, which yield the results $\lambda(\mathrm{OH})=-7.547$,[12] and $\lambda(\mathrm{OD})=-14.10$.[13] In rough agreement with our observations of the Zeeman effect, these values are in fact about 1% larger than those measured by DST (although they are considered[1] to be uncertain by nearly the same amount). On the basis of this optical evidence, and lacking more precise evidence to the contrary, we conclude that sufficient faith cannot be placed in the wave functions to allow one to regard the $g$-factor discrepancies in Table IV as significant.

Another, less serious, point of disagreement between this experiment and that of DST exists in the hfs measurements; this is illustrated by Table VI, where the value of $|A_1|$ measured by DST for the $^2\Pi_{\frac{3}{2}}$, $J=9/2$ level is seen to be somewhat inconsistent with the values of $a$, $b$, and $c$ derived here. In the face of recognized theoretical errors originating in the neglect of off-diagonal hfs interactions, this disagreement probably has only marginal significance. The over-all consistency of the hfs measurements with the theory of Frosch and Foley is quite satisfying.

The size of the relativistic hfs interaction, surprisingly large, might have been predicted from recent electron paramagnetic resonance studies of $\gamma$- and $\beta$-irradiated ice.[29] There a trapped radical species is found, identified as OH by isotopic substitution, that yields a simple two-line spectrum centered near the position of the spin resonance of free electrons. Apparently, interactions with the solid "quench" the electronic orbital angular momentum of the trapped radicals, leaving a single Kramers-type doublet as the ground electronic level. In the resulting absence of a strong spin-orbit coupling of the electron spin to the molecular axis, the first order hfs interaction should be isotropic, represented by $AI_ZS_Z$, where the $Z$ axis is fixed by the applied magnetic field. Both the relativistic and the dipole-dipole interactions contribute to the coupling constant $A$ but, as in the free radical, the dipole-dipole contribution should be small, probably less than 15 Mc/sec, because of the relatively large separation of the unpaired electron distribution from the hydrogen nucleus. The measured hfs coupling constant of the trapped radical is $110\pm5$ Mc/sec; clearly the relativistic interaction is responsible for most of this. The experimental equality of this value with the measured relativistic interaction in the free radical is rather suggestive, but without more definite information on the dipole-dipole interaction in the trapped radical the two values should not be compared too closely. Nevertheless, the hfs measurements of the present experiment lend strong support to the identification of the paramagnetic centers in irradiated ice as trapped OH radicals.

In spite of the considerable intensity of the absorption spectra observed both here and in the experiment of DST it seems clear that the concentration of OH radicals in the products of an electric discharge in water vapor is, at least in our case, really very small, much less than the lower limit of 3% estimated by DST. This conclusion follows directly from the undetectability of the OH magnetic dipole spectrum under conditions where the atomic hydrogen absorption signals are roughly 3000 times the spectrometer noise level. If one assumes an atomic hydrogen concentration as high as 50%, and allows for differences in linewidths, level populations and magnetic moments, an upper limit for the OH concentration, under optimum pressure and discharge conditions, would be about 1%. The fractional condensation experiments described in Sec. II, in which the width of the OH absorption lines was found to be independent of their intensity, are consistent with this estimate. Further support is provided by earlier intensity measurements on the ultraviolet absorption by OH,[30] the radicals again produced by an electric discharge in water vapor: for a total pressure of 1 mm Hg the partial pressure of OH was estimated to be $10^{-3}$ mm Hg. Since the concentration estimates of DST depend critically on the value used for the electric dipole moment of OH, it appears likely that the true value is somewhat larger than 1.5 Debye units, the value used in their estimates; theoretical predictions[26] of the electric moment range from 2 to 3 Debye units.

[29] S. Siegel, L. H. Baum, S. Skolnik, and J. M. Flournoy, J. Chem. Phys. **32**, 1249 (1960); L. H. Piette, R. C. Rempel, H. E. Weaver, and J. M. Flournoy, J. Chem. Phys. **30**, 1623 (1959); R. Livingstone, H. Zeldes, and E. H. Taylor, Discussions Faraday Soc. **19**, 166 (1955).

[30] O. Oldenberg and F. F. Rieke, J. Chem. Phys. **6**, 439 (1938).